ANIMAL MODEL OF METASTATIC PHEOCHROMOCYTOMA: EVALUATION BY MRI AND PET

MARTINIOVA L[1,6], LAI EW[1], THOMASSON D[2], KIESEWETTER DO[3], SEIDEL J[4], MERINO MJ[5], KVETNANSKY R[6], PACAK K[1]

[1]Reproductive and Adult Endocrinology Program, Eunice Kennedy Shriver National Institutes of Child Health and Human Development, Bethesda, MD, 20892, USA; [2] Laboratory of Diagnostic Radiology, Warren Grant Magnuson Clinical Center, Bethesda, MD, 20892, USA; [3] Positron Emission Tomography Radiochemistry Group, National Institute of Biomedical Imaging and Bioengineering, Bethesda, MD, 20892, USA; [4] Molecular Imaging Program, National Cancer Institute, Bethesda, MD, 20892, USA; [5] Laboratory of Pathology, National Cancer Institute, Bethesda, MD, 20892, USA; [6] Institute of Experimental Endocrinology, Slovak Academy of Sciences, Bratislava, Slovakia, 83306
e-mail: karel@mail.nih.gov

Objective. The development of metastatic pheochromocytoma animal model provides a unique opportunity to study the physiology of these rare tumors and to evaluate experimental treatments. Here, we describe the use of small animal imaging techniques to detect, localize and characterize metastatic lesions in nude mice.

Methods. Small animal positron emission tomography (PET) imaging and magnetic resonance imaging (MRI) were used to detect metastatic lesions in nude mice following intravenous injection of mouse pheochromocytoma cells. [18F]-6-fluoro-dopamine ([18F]-DA) and [18F]-L-6-fluoro-3,4-dihydroxyphenylalanine, which are commonly used for localization of pheochromocytoma lesions in clinical practice, were selected as radiotracers to monitor metastatic lesions by PET.

Results. MRI was able to detect liver lesions as small as 0.5mm in diameter. Small animal PET imaging using [18F]-DA and [18F]-DOPA detected liver, adrenal gland, and ovarian lesions.

Conclusion. We conclude that MRI is a valuable technique for tumor growth monitoring from very early to late stages of tumor progression and that animal PET confirmed localization of metastatic pheochromocytoma in liver with both radiotracers.

Key words: Anatomical imaging – Functional imaging – MRI, small animal PET – Animal model

In pre-clinical oncology, there is currently a strong focus on the development of animal models of human cancer to study experimental treatment therapies. Before testing any kind of experimental drugs, it is important to develop a suitable animal model that is physiologically and patho-logically similar to the human disease. Moreover in monitoring the responses to therapy, anatomical imaging may yield non-specific findings and functional or metabolic changes which occur without corresponding anatomical correlates may be missed (TOWNSEND 2008).

Corresponding author: Karel Pacak, MD, PhD, DSc, Professor of Medicine, NICHD, NIH, Building 10 Room 1E-3140, 10 Center Drive MSC-1109, Bethesda, Maryland, 20892-1109 USA, E-mail: karel@mail.nih.gov, Phone: 301-402-4594, Fax: 301-402-4712, e-mail: karel@mail.nih.gov

Abbreviations: PET – positron emission tomography; MPC – mouse pheochromocytoma cell; i.v. – intravenous; SUV_{max} – the maximum standardized uptake value, 2D-OSEM – 2-dimensional ordered-subsets expectation maximum, [18F]-DA – [18F]-6-fluoro-dopamine, [18F]-DOPA – [18F]-L-6-fluoro-3,4-dihydroxyphenylalanine

Subcutaneous mouse tumor models are most common in cancer research studies since the tumors are usually visible and physically accessible. Conversely, metastatic animal tumor models, where tumors are potentially spread throughout the body, require non-invasive methods to localize the metastases, monitor growth, and evaluate therapeutic response. Small animal imaging systems developed during the past few years have these characteristics.

Small animal high-resolution magnetic resonance imaging (MRI) scanners, for example, allow imaging of the anatomy of living mice with appreciation of soft tissue contrast. However, its application in visualizing organs and organ lesions inside the abdominal cavity has been hampered because of the animal's high respiration/heart rates and increased magnetic susceptibility and motion artifacts (Cheung et al. 2008). Small animal positron emission tomography (PET) scanners have been developed to perform functional imaging in small animals. Since the dimensions of mouse organs compared to humans are very small, MRI and (particularly) PET technology have been advanced dramatically compared to human imaging systems to achieve the required levels of performance necessary for this task. It should also be recalled that unlike MRI studies, PET studies require administration of an endogenous tissue-specific radio-pharmaceutical, so that each individual study requires synthesis of a labeled compound.

In the present study, we used a clinical MRI scanner and small animal PET scanner to localize metastatic pheochromocytoma in nude mice. Pheochromocytoma tumors are rare neuroendocrine tumors arising from chromaffin cells (Lloyd et al. 2004; Pacak et al. 2004). The adrenal medulla is the primary origin of these tumors (80-85 %), with the remainder arising from extra-adrenal chromaffin tissue (Lenders et al. 2005). It is estimated that over 25 % of pheochromocytomas are malignant (Eisenhofer et al. 2004). To date, there is no accurate prognostic marker for malignant pheochromocytoma (Eisenhofer et al. 2004).

The biochemical properties of metastatic tumors present the possibility of targeting lesions with different radiotracers. Animal MPC cell lines resemble human normal and neoplastic chromaffin cells closely as they express phenylethanolamine-N-methyltransferase (PNMT), as opposed to the rat PC12 cell line, which does not (Greene et al. 1976). PNMT is an enzyme found in the adrenal medulla that converts norepinephrine to epinephrine. Both pheochromocytoma cell lines, MPC and PC12, express tyrosine hydroxylase (TH), the enzyme

responsible for catalyzing the conversion of amino acid L-tyrosine to dihydroxyphenylalanine (DOPA). DOPA is a precursor for dopamine (DA), which in turn is a precursor for the catecholamines secreted most often in excess in patients with pheochromocytoma, norepinephrine and epinephrine. A specific radiopharmaceutical, [^{18}F]-6-fluoro-dopamine ([^{18}F]-DA) enters cells via the membrane norepinephrine transporter translocated and then stored in vesicles via the vesicular monoamine transporter where the radioactivity is concentrated (Pacak et al. 2001). Another PET agent used for localization of pheochromocytoma is [^{18}F]-L-6-fluoro-3,4-dihydroxy-phenylalanine ([^{18}F]-DOPA) (Luxen et al. 1990). According to previous studies, [^{18}F]-DOPA PET is highly sensitive and specific for the detection of pheochromocytoma (Hoegerle et al. 2002). Both of these agents were used in the studies described below.

Materials and Methods

Animal studies. All animal experiments were performed with the approval of the NIH Institutional Animal Care and Use Committee. Un-anesthetized adult (six to eight weeks) female athymic nude mice (NCr-nu, Taconic, Germantown, NY, USA) were injected by tail vein with 1×10^6 mouse pheochromocytoma cells (MPC 4/30PRR) to create in vivo metastatic pheochromocytoma (Martiniova et al. 2009a).

Magnetic resonance imaging. All tumor bearing mice (n = 5) were scanned by MRI 3-4 weeks after i.v. injection of MPC cells. A 3 Tesla MRI clinical scanner (Intera, Philips Medical System, Best, Netherlands) using a dedicated 40 mm solenoid coil (Philips, Best, Netherlands) and the following data acquisition parameters: field-of-view (FOV), data matrix 512×512, 40 slices, TR/TE 5000/65 milliseconds, flip angle 90º/180º, slice thickness 0.5 mm, 0.156×0.156 mm^2 in-plane resolution was used as previously described (Martiniova et al. 2009b). A respiratory triggered T$_2$-weighted MRI technique was chosen based on its high signal-to-noise ratio (SNR) without the need for contrast media.

Small animal PET imaging. [^{18}F]-DA and [^{18}F]-DOPA PET were performed 24 hours apart. Anesthetized mice were injected with approximately 3.5-3.9 MBq of [^{18}F]-DA and 3.4-3.8 MBq of [^{18}F]-DOPA via the tail vein. PET scans were performed using the Advanced Technology Laboratory Animal Scanner, (ATLAS) PET scanner (Seidel 2003). The scanner has a computer controlled animal bed with a transverse field-of-view of 6.8 cm, an axial FOV of two cm and acquires data exclusively in
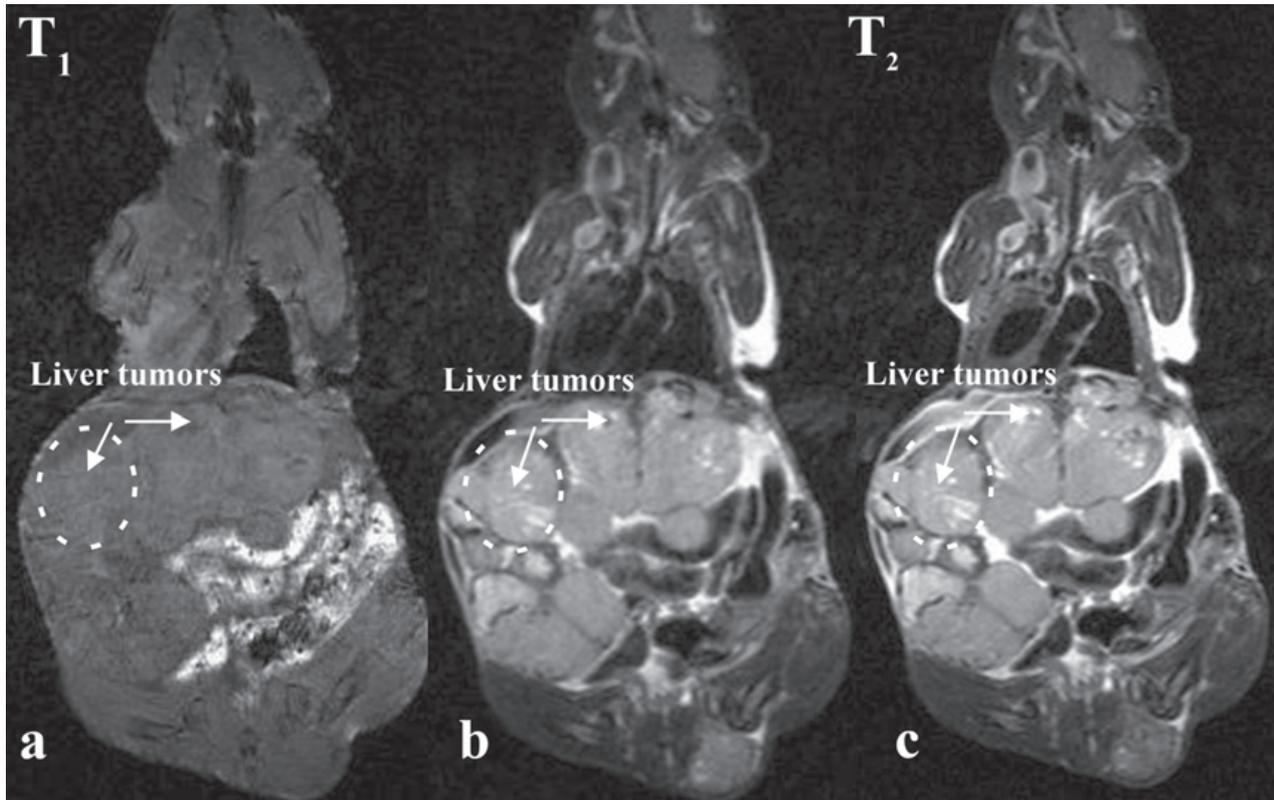
Fig. 1 Comparison of T$_1$-weighted (a) and T$_2$-weighted images without (b) and with respiratory triggering (c). The T$_1$-weighted imaging protocol is not suitable for localization of liver lesions. T$_2$-weighted image provides good contrast to liver tumors. Improved contrast-to-noise ratio was achieved using respiratory triggering.

3-D. The reconstructed voxel size was 0.56×0.56×1.125 mm^3. The spatial resolution of this system is 1.8 mm full-width at half-maximum (FWHM) in the central FOV. Mice were positioned in the prone position on a heated animal bed near the center of the FOV of the ATLAS scanner, the region with the highest image resolution and sensitivity. Dynamic data acquisition (one frame/10 min, up to 6 frames) were started about 1 min after radio-tracer injection and whole body images (2-3 bed positions, each 15 min) were obtained immediately after the dynamic acquisition. All acquisitions were performed with a 100-700 keV energy window. The images were reconstructed using a 2-dimensional ordered-subsets expectation maximum (2D-OSEM) algorithm and no corrections were applied for attenuation or scatter. For each scan, regions of interest (ROI) were drawn over the tumor, normal tissue, and major organs. The maximum radioactivity accumulation within the tumors or organs was obtained from mean pixel values within the multiple ROIs. The results were calculated as a percentage injected dose per gram (%ID/g) and SUV (standardized uptake value). We used also the maximal uptake within the tumor obtained from the most active voxel cluster located within the ROI. This is equivalent to the maximum standardized uptake value (SUV$_{max}$) used in clinical PET studies (ALIAGA et al. 2007) that minimize the partial volume effect (KEYES 1995).

Necropsy and histopathology. Animals were sacrificed with cervical dislocation at the end of the last imaging study. An autopsy was performed and organs and bones were carefully examined. Tumor tissue was removed; small pieces of tumors were immediately frozen on dry ice and stored at -80 ºC. The presence of metastatic pheochromocytoma lesions was further characterized by histopathological examination.

Results

Magnetic resonance imaging. All animals developed liver lesions (5/5), adrenal gland metastases occurred in
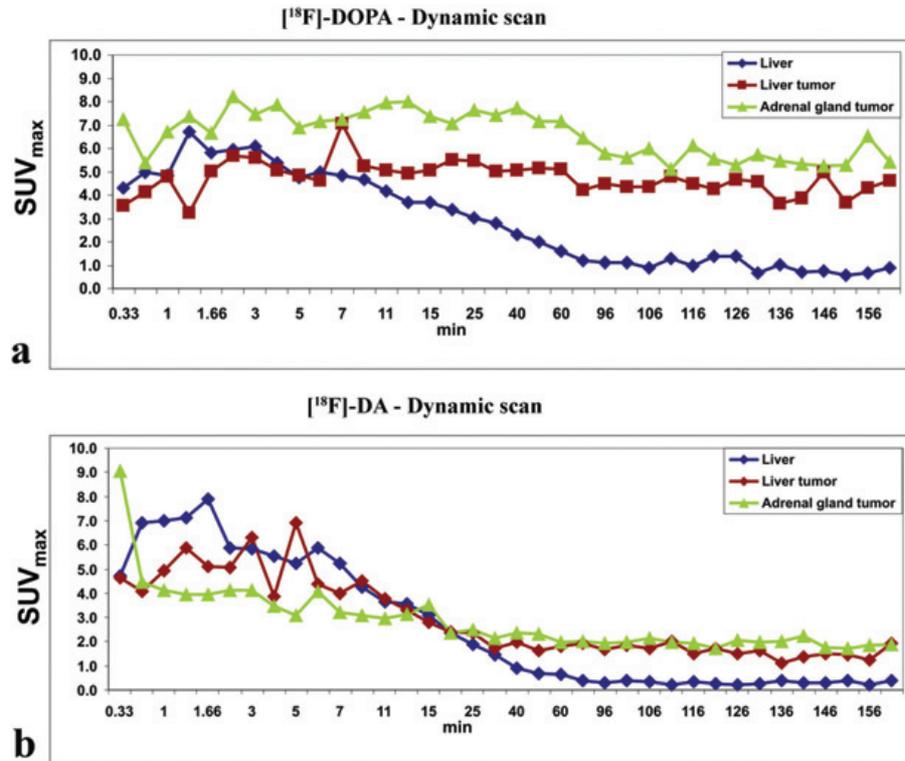
Fig. 2 Dynamics of [18F]-DOPA (a) and [18F]-DA (b) liver, liver and adrenal gland tumors uptake. Time–activity curves start approximately 1 min after i.v injection of tracer and capture uptake up to 160 min. The plateau in liver, liver and adrenal tumors after 60 min is the most suitable time for monitoring tumors since the tumor-to-background ratio is the highest.
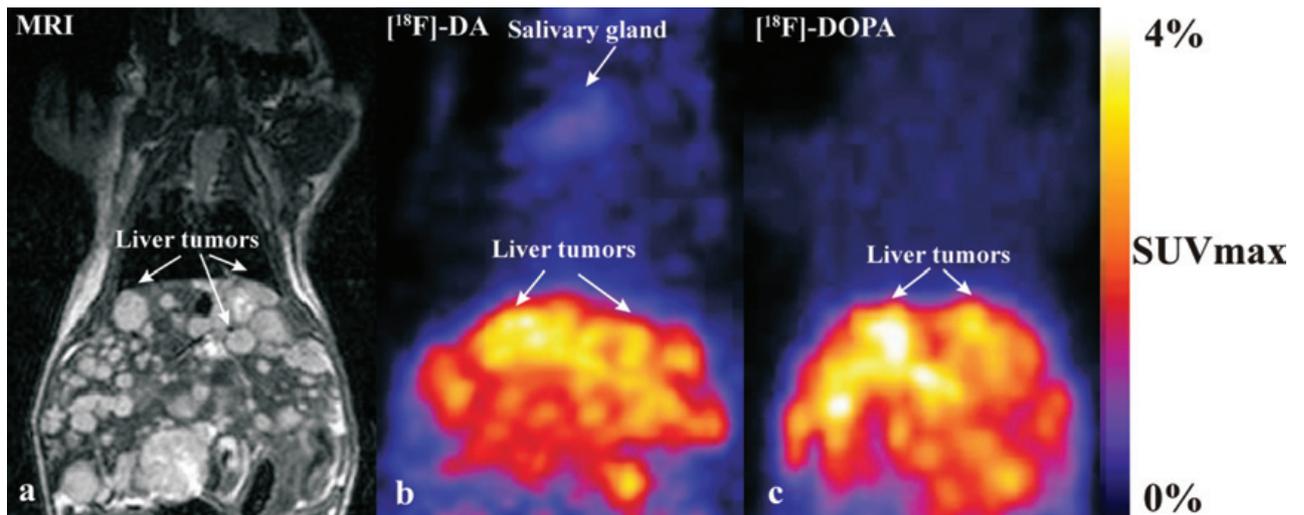

Fig. 3 Numerous liver lesions are visualized by MRI (a), [18F]-DA (b) and [18F]-DOPA (c) in the same mouse. In the MRI image, liver lesions are visible from 0.5 mm up to 5 mm, due to the high special resolution and signal-to-noise ratio. [18F]-DA uptake is also present in the salivary glands and kidneys. Liver lesions are observed in liver with both radiotracers.

(2/5), ovarian and lung metastases in (1/5) and kidney and bone metastases in (1/5). Representative MR images are shown on Figure 1. T_1 (Figure 1a) and T_2- weighed (Figure 1b, c) images with and without respiration triggering demonstrate liver tumor visualization. MRI with respiratory triggering allowed more accurate detection of small liver lesions (0.5 mm in diameter) as early as 20 days after i.v MPC cells injection. Liver lesions without respiratory triggering were detected as small as 1mm in diameter. Finally, detection of lung and kidney lesions was possible only using respiration triggering.

Small animal PET. Mice with metastatic lesions developed after i.v. injection were first scanned on MRI to initially localize lesions and then imaged with PET approximately 30 days after i.v injection, when liver lesions were larger than 4mm in diameter. Since the pharmacokinetics of [^{18}F]-DA and [^{18}F]-DOPA was unknown in pheochromocytoma lesions, dynamic scans were performed up to 160 minutes after i.v injection of both compounds (Figure 2). The uptake of both compounds in the liver, liver lesions, and adrenal gland lesions was evaluated. Notably, the uptake plateau appeared after 60 minutes with both compounds. Thus, it is the best time for characterization of liver and adrenal lesions, because the uptake ratio in tumors versus liver was the highest. As a result, all subsequent whole-body images were acquired 60 minutes after i.v injection of both compounds.

In general, liver lesions were detected well with both radio-pharmaceuticals, as were adrenal gland lesions. Liver lesions were evaluated from whole-body scans. [^{18}F]-DOPA SUV$_{max}$ of liver was 1.2 ± 0.2 (mean $\pm$ SEM) and ranging 3-5 SUV$_{max}$ in liver lesions. [^{18}F]-DA SUV$_{max}$ of liver was 0.8 ± 0.18 (mean $\pm$ SEM) and ranging 1.5-2 in liver lesions. Lung and ovarian lesions were visible only if larger than 4mm with [^{18}F]-DOPA. [^{18}F]-DA and [^{18}F]-DOPA studies were performed on subsequent days, and high uptake in liver tumors demonstrated physiological activity of pheochromocytoma liver lesions (5/5) as well as adrenal (2/5) and ovarian (1/5) lesions. However, [^{18}F]-DA and [^{18}F]-DOPA uptake also presented in other organs surrounding liver lesions (liver, kidney, pancreas, gall bladder) (Figure 3). The number of liver lesions was not always possible to determine. The kidney lesions were usually too small to detect with PET. Histopathology confirmed appearance of all lesions found on MRI and PET. An example of a comparison of anatomical and functional imaging is presented on Figure 3, where liver lesions were localized by MRI at day 38 after MPC cells injection.

Discussion

This study utilized multimodality imaging methods for localization of metastatic pheochromocytoma lesions in nude mice. MRI is an appropriate technique for visualization of mouse anatomy and organ lesions. Liver, adrenal, and ovarian metastatic lesions are successfully confirmed and visualized by functional imaging using [^{18}F]-6F-DA and [^{18}F]-DOPA PET, demonstrating that both compounds are suitable for localizing mouse pheochromocytoma.

MRI has been proposed as an effective alternative to computed tomography (CT). It has even been suggested that, for characterization of human adrenal masses, MRI is superior to CT (HONIGSCHNABL et al. 2002). In the present study, the MRI SNR was sufficient to allow visualization of very small lesions without use of gadolinium contrast agent. Although small animal PET scanners can reveal biological function and the efficacy of putative therapeutic agents, visualization of metastatic lesions by functional imaging can be very challenging due to spatial resolution limitation. However, if the size of lesions is around 4mm (twice the scanner resolution) in diameter, both [^{18}F]-DA and [^{18}F]-DOPA are able to detect liver and adrenal gland lesions after a 60 minute uptake interval. Liver does not have a storage mechanism for [^{18}F]-DA and [^{18}F]-DOPA and thus liver activity was low at 60 minutes post injection compared to lesions. Liver pheochromocytoma lesions are characterized by granular vesicles where the storage of both compounds is significant.

New small animal imaging systems are now available that combine radionuclide imaging with anatomical imaging in the same machine, e.g. PET with CT, SPECT with CT, etc. so that the image data acquired in the same animal by both methods can be accurately superimposed with image fusion software. This technique, which is being used increasingly in the diagnosis and staging of human disease (TOWNSEND 2008) will very likely also improve evaluation of metastatic tumor models. For example, CT or MRI could provide anatomical imaging and both could also be used for attenuation correction and thus improve the quality of the radionuclide image data. Our study suggests that multimodality imaging by MRI and small animal PET in animal models of metastatic pheochromocytoma may be a particularly useful combination provided that cost and performance issues can be overcome.

Acknowledgements

We would like to acknowledge the valuable assistance of the colleagues in our group; we thank Dr. Graeme EISENHOFER for help with catecholamine assay and Mr. Danny SOLIS for his assistance with animals. We thank Dr. Marcelino BERNARDO for guidance and support with anatomical imaging. Special thanks belong to Michael V. GREEN for his great support and valuable suggestions. This research was supported (in part) by the Intramural Research Program of the NIH including NICHD, CC, NCI, and APVV-0148-06 (to R.K.).The authors have no conflict of interest to disclose.

References

ALAVI A, MAVI A, BASU S, FISCHMAN A: Is PET-CT the only option? Eur J Nucl Med Mol Imaging 34, 819–821, 2007

ALIAGA A, ROUSSEAU JA, CADORETTE J, CROTEAU E, VAN LIER JE, LECOMTE R, BENARD F: A small animal positron emission tomography study of the effect of chemotherapy and hormonal therapy on the uptake of 2-deoxy-2-[F-18]fluoro-D-glucose in murine models of breast cancer. Mol Imaging Biol **9**, 144–150, 2007

Cheung JS, Guo H, Leung JC, Man K, Lai KN, Wu EX: MRI visualization of rodent liver structure and peritoneal adhesion with dialyzate enhancement. Magn Reson Med **59**, 1170–1174, 2008

Eisenhofer G, Bornstein SR, Brouwers FM, Cheung NK, Dahia PL, de Krijger RR, Giordano TJ, Greene LA, Goldstein DS, Lehnert H, Manger WM, Maris JM, Neumann HP, Pacak K, Shulkin BL, Smith DI, Tischler AS, Young WF, Jr.: Malignant pheochromocytoma: current status and initiatives for future progress. Endocr Relat Cancer **11**, 423–436, 2004

Green MV, Seidel J, Vaquero JJ, Jagoda E, Lee I, Eckelman WC: High resolution PET, SPECT and projection imaging in small animals. Comput Med Imaging Graph **25**, 79–86, 2001

Greene LA, Tischler AS: Establishment of a noradrenergic clonal line of rat adrenal pheochromocytoma cells which respond to nerve growth factor. Proc Natl Acad Sci USA **73**, 2424–2428, 1976

Hoegerle S, Nitzsche E, Altehoefer C, Ghanem N, Manz T, Brink I, Reincke M, Moser E, Neumann HP: Pheochromocytomas: detection with 18F DOPA whole body PET--initial results. Radiology **222**, 507–512, 2002

Honigschnabl S, Gallo S, Niederle B, Prager G, Kaserer K, Lechner G, Heinz-Peer G: How accurate is MR imaging in characterisation of adrenal masses: update of a long-term study. Eur J Radiol **41**, 113–122, 2002

Keyes JW, Jr.: SUV: standard uptake or silly useless value? J Nucl Med **36**, 1836–1839, 1995

Lenders JW, Eisenhofer G, Mannelli M, Pacak K: Phaeochromocytoma. Lancet **366**, 665–675, 2005

Lloyd RV, Tischler AS, Kimura N: Pathology and Genetics of Tumours of Endocrine Organs World Health Organization Classification of Tumors, 136–146, 2004

Luxen A, Perlmutter M, Bida GT, Van Moffaert G, Cook JS, Satyamurthy N, Phelps ME, Barrio JR: Remote, semiautomated production of 6-[18F]fluoro-L-dopa for human studies with PET. Int J Rad Appl Instrum [A] **41**, 275–281, 1990

Martiniova L, Lai EW, Elkahloun AG, Abu-Asab M, Wickremasinghe A, Solis DC, Perera SM, Huynh TT, Lubensky IA, Tischler AS, Kvetnansky R, Alesci S, Morris JC, Pacak K: Characterization of an animal model of aggressive metastatic pheochromocytoma linked to a specific gene signature. Clin Exp Metastasis 26, 239–250, 2009a

Martiniova L, Kotys S, Thomasson D, Schimel D, Lai E: Non-invasive monitoring of a murine model of metastatic pheochromocytoma: a comparison of contrast enhanced microCT and non-enhanced MRI. J Magn Reson Imaging **29**, 685–691, 2009b

Mayo-Smith WW, Boland GW, Noto RB, Lee MJ: State-of-the-art adrenal imaging. Radiographics **21**, 995–1012, 2001

Pacak K, Eisenhofer G, Carrasquillo JA, Chen CC, Li ST, Goldstein DS: 6-[18F]fluorodopamine positron emission tomographic (PET) scanning for diagnostic localization of pheochromocytoma. Hypertension 38, 6–8., 2001

Pacak K, Eisenhofer G, Goldstein DS: Functional imaging of endocrine tumors: role of positron emission tomography. Endocr Rev **25**, 568–580, 2004

Powers JF, Evinger MJ, Tsokas P, Bedri S, Alroy J, Shahsavari M, Tischler AS: Pheochromocytoma cell lines from heterozygous neurofibromatosis knockout mice. Cell Tissue Res **302**, 309–320, 2000

Seidel J: Resolution uniformity and sensitivity of the NIH ATLAS small animal PET scanner: comparison to simulated LSO scanners without depth-of-interaction capability. IEEE Trans Nuc Sci **50**, 1347–1350, 2003

Townsend DW: Multimodality imaging of structure and function. Phys Med Biol **53**, R1-R39, 2008